



# Hydrogenation of CO<sub>2</sub> to alcohol species over Co@Co<sub>3</sub>O<sub>4</sub>/C-N catalysts

Yun Lian, Tingfeng Fang, Yuhua Zhang, Bing Liu\*, jinlin Li\*



Key Laboratory of Catalysis and Energy Materials Chemistry of Ministry of Education & Hubei Key Laboratory of Catalysis and Materials Science, South-Central University for Nationalities, Wuhan 430074, China

## ARTICLE INFO

### Article history:

Received 7 August 2019

Revised 9 September 2019

Accepted 10 September 2019

### Keywords:

CO<sub>2</sub> hydrogenation

Alcohol synthesis

ZIF-67

Co@Co<sub>3</sub>O<sub>4</sub>/C-N catalysts

## ABSTRACT

Co/C-N materials were synthesized with calcination of ZIF-67 at a N<sub>2</sub> atmosphere. Co@Co<sub>3</sub>O<sub>4</sub>/C-N catalysts were prepared by partially oxidized of Co/C-N in air under different conditions. The catalysts were characterized with XRD, BET, TEM, TGA, H<sub>2</sub>-TPD, ESR and XPS. The metallic Co in Co/C-N was the main activity site for the CO<sub>2</sub> hydrogenation as it supplied dissociative hydrogen on the surface. Partial oxidation of Co/C-N decreased the content of metallic Co, decreasing the amount of dissociative H<sub>2</sub> and thus the CO<sub>2</sub> conversion, while increasing the methanol selectivity. Oxygen defects in Co@Co<sub>3</sub>O<sub>4</sub>/C-N improved the dissociation of CO<sub>2</sub> and helped to produce desired alcohol species. The highest yield of MeOH, 2.0 mmol g<sup>-1</sup> h<sup>-1</sup>, was obtained over Co@Co<sub>3</sub>O<sub>4</sub>/C-N (250, 2 h) at 220 °C.

© 2019 Elsevier Inc. All rights reserved.

## 1. Introduction

Carbon dioxide is the main greenhouse gas produced in many industrial processes. The efficient utilization of CO<sub>2</sub> to produce fuel and high value chemicals has been drawing researchers' attention [1]. Alcohol species synthesis from CO<sub>2</sub> hydrogenation (CO<sub>2</sub> + 3H<sub>2</sub> → CH<sub>3</sub>OH + H<sub>2</sub>O, 2CO<sub>2</sub> + 6H<sub>2</sub> → C<sub>2</sub>H<sub>5</sub>OH + 3H<sub>2</sub>O), are highly attractive products as they are widely used as intermediates in many chemical industries, and are also transportable fuels to replace petroleum [2]. For the CO<sub>2</sub> hydrogenation, various catalytic systems based on Cu [3], Co [4] Pd [5] have been studied. Methanol synthesis by CO<sub>2</sub> hydrogenation on Cu based catalysts was usually accompanied with undesired CO formation via reverse water gas shift reaction (CO<sub>2</sub> + H<sub>2</sub> → CO + H<sub>2</sub>O, RWGS) [6]. Co based catalysts have been extensively studied for the Fischer-Tropsch synthesis reaction. However, methane was the main product in CO<sub>2</sub> hydrogenation process due to the strong hydrogenation ability of metallic Co [7]. Somorjai et al. found cobalt oxides performed better than fully reduced cobalt supported on TiO<sub>2</sub> in CO<sub>2</sub> hydrogenation, for CoO<sub>x</sub> and partially encapsulated metallic Co formed some unique active sites [8]. In our earlier research, the system formed with partially reduced mesoporous Co<sub>3</sub>O<sub>4</sub> and metallic Co nanoparticles was shown to be the active site to produce alcohol's by CO<sub>2</sub> hydrogenation [9].

Nitrogen-doped carbon-supported metal catalysts have also recently gained considerable attention. The incorporation of nitrogen in the carbon architecture played multiple roles to improve the catalytic activity such as the stabilization of metal nanoparticles

and the enhancement of the electron transfer ability [10]. In CO<sub>2</sub> hydrogenation reaction, the basic nitrogen improved the adsorption of CO<sub>2</sub>, and enhanced the catalytic activity [11]. ZIF-67 (ZIF: zeolitic imidazolate framework), which is composed of cobalt cation's and 2-methylimidazole ligand's, would be a promising precursor for the preparation of nitrogen-doped carbon supported cobalt catalysts. Herein, nitrogen-doped carbon-supported cobalt catalysts (Co/C-N) were prepared by the polymerization of ZIF-67. Furthermore, the partially oxidized catalysts (Co@Co<sub>3</sub>O<sub>4</sub>/C-N) were also prepared for comparison. To the best of our knowledge, this application of Co@Co<sub>3</sub>O<sub>4</sub>/C-N in CO<sub>2</sub> hydrogenation reaction is unprecedented.

## 2. Experimental section

### 2.1. Catalyst preparation

Co/C-N catalysts were prepared by the calcination of ZIF-67. Briefly, 2.16 g of Co(NO<sub>3</sub>)<sub>2</sub>·6H<sub>2</sub>O and 4.88 g of 2-methylimidazole were dissolved in 150 mL methanol separately. The solution of 2-methylimidazole was added dropwise into the solution of cobalt nitrate. Then the mixture was stirred for 6 h at room temperature. The obtained purple suspension was centrifuged and washed with methanol for three times. The ZIF-67 was obtained by drying the purple solid at 80 °C overnight, and then calcined at 600 or 800 °C for 6 h in N<sub>2</sub> atmosphere. The as-prepared catalysts are denoted as Co/C-N-600 and Co/C-N-800.

Co@Co<sub>3</sub>O<sub>4</sub>/C-N catalysts were prepared by the oxidation of Co/C-N-600 in air at 220 or 250 °C for 2 h or 6 h. The as-prepared catalysts are denoted as Co@Co<sub>3</sub>O<sub>4</sub>/C-N (220, 2 h), Co@Co<sub>3</sub>O<sub>4</sub>/C-N (250, 2 h) and Co@Co<sub>3</sub>O<sub>4</sub>/C-N (250, 6 h) respectively.

\* Corresponding authors.

E-mail addresses: [liubing@mail.scuec.edu.cn](mailto:liubing@mail.scuec.edu.cn) (B. Liu), [jinlinli@aliyun.com](mailto:jinlinli@aliyun.com) (j. Li).

## 2.2. Catalyst characterization

The powder X-ray diffraction (XRD) patterns were recorded on an automated powder X-ray diffractometer (40 kV, 40 mA, Bruker-D8) using a Cu K $\alpha$  radiation source ( $\lambda = 1.54056 \text{ \AA}$ ) in the range of 10–80° with step size of 2°/min.

The surface area and pore volume were measured with low-temperature nitrogen adsorption/desorption (77 K, Quantachrome Autosorb-1-C-MS). The specific surface area was determined from the linear portion of the standard Brunauer-Emmett-Teller (BET) plot. The total pore volumes and the average pore sizes were calculated from the desorption branch of the adsorption isotherm using the Barrett-Joyner-Halenda (BJH) formula. Before the adsorption measurements, the sample was degassed at 350 °C under vacuum for 3 h. The pressure range used for the BET measurements was 9.849–100.566 kPa.

The ability of CO<sub>2</sub> adsorption for the catalyst was measured by CO<sub>2</sub>-temperature program desorption (CO<sub>2</sub>-TPD) experiment. Prior to adsorption of CO<sub>2</sub>, the sample (100 mg) was pretreated at 300 °C for 1 h and cool 100 °C in flowing Ar. At this temperature, sufficient CO<sub>2</sub> (30 mL min<sup>-1</sup>) was injected at least 30 min until adsorption saturation, followed by purging with Ar (30 mL min<sup>-1</sup>) for about 1 h. The temperature was then raised from 100 to 650 °C at a ramp rate of 10 °C min<sup>-1</sup> to desorb CO<sub>2</sub>. The desorbed CO<sub>2</sub> was detected by on-line gas chromatography with a TCD detector.

H<sub>2</sub>-temperature program desorption (H<sub>2</sub>-TPD) experiments were carried out using AMI-200 from Zeton Altamira Company. For each measurement, about 50 mg of the catalyst was placed in a quartz tube reactor and reduced at 220 °C for 2 h using a flow of high-purity hydrogen (>99.999%, 30 mL min<sup>-1</sup>) and then cooled from 220 °C to 50 °C in flowing hydrogen. Then hydrogen was switched to high-purity Ar (>99.999%, 25 mL min<sup>-1</sup>) for 30 min. Subsequently, the sample was heated from 50 °C to 600 °C at a rate of 10 °C min<sup>-1</sup> and kept at 600 °C for 2 h in a flow of Ar (25 mL min<sup>-1</sup>). The desorbed H<sub>2</sub> was monitored by TCD and used for quantification.

Thermogravimetric analysis (TGA) was carried out on a NETZSCH TG 209F3 instrument. The sample (~10 mg) was placed in a ceramic crucible and heated from 30 to 700 °C with a ramp rate of 10 °C min<sup>-1</sup> under air (flow rate 30 mL min<sup>-1</sup>).

X-ray photoelectron spectroscopy (XPS) was conducted on a Thermo VG scientific ESCA MultiLab-2000 spectrometer with a monochromatized Al K $\alpha$  source (1486.6 eV) at a constant analyzer pass energy of 25 eV. The binding energy was estimated to be accurate within 0.2 eV. Co 2p, N 1s and O 1s spectra were acquired, C 1s was set at 284.6 eV and taken as a reference for binding energy (BE) calibration. The software XPS PEAK was used to fit the XPS spectra using a mixture of Gaussian and Lorentzian functions in a 40/60 ratio and a Shirley background.

Electron spin resonance (ESR) signals of radicals, trapped by a spin-trap reagent DMPO (5,5-dimethyl-1-pyrroline-N-oxide) in water, were examined on a Bruker model JEOL JES-FA200 spectrometer equipped with a Quanta-Ray Nd: YAG laser system as the irradiation source ( $\lambda \geq 420 \text{ nm}$ ). To minimize experimental errors, the same type of quartz capillary tube was used for all ESR measurements.

## 2.3. Typical procedure of CO<sub>2</sub> hydrogenation

All catalytic tests were performed in a fixed-bed stainless steel mini-reactor (length of 53 cm and inside diameter of 8 mm). A mixed feed gas (22.5% CO<sub>2</sub>, 67.5% H<sub>2</sub> and 10% N<sub>2</sub>) was used without further purification. The pressure of the reactor was controlled with a backpressure regulator. For each experiment, the catalyst to be tested (0.2 g) was mixed with 0.2 g of silica. The system was pressurized to 2 MPa by feeding the mixed gas at

20 mL/min. The reaction for each catalyst was kept for 50 h at 200 °C or 250 °C and GHSV = 6 L h<sup>-1</sup> g<sub>cat</sub><sup>-1</sup>. The gas products were analyzed on line by an Agilent GC3000 gas chromatography (thermal conductivity and flame ionization detectors). The liquid products were collected in a cold trap and analyzed with a 4890 gas chromatography (flame ionization detectors) off line. The reaction parameters of CO<sub>2</sub> conversion, selectivity and space time yield (STY) are defined as below (where MeOH refers to methanol)

$$X_{\text{CO}_2} = \frac{n_{\text{CO}_2, \text{in}} - n_{\text{CO}_2, \text{out}}}{n_{\text{CO}_2, \text{in}}}, \quad \text{selectivity} = \frac{n_{\text{product, out}} \times \text{carbon number}}{n_{\text{CO}_2, \text{out}}}$$

$$\text{STY}_{\text{MeOH}} = \frac{\text{FCO}_2, \text{in} \times X_{\text{CO}_2} \times 60 \times S_{\text{MeOH}}}{22.4 \times M_{\text{cat}}}$$

## 3. Results and discussion

The X-ray diffraction patterns of Co/C-N catalysts are shown in Fig. 1. The XRD patterns of Co/C-N showed the peaks with 2 $\theta$  at

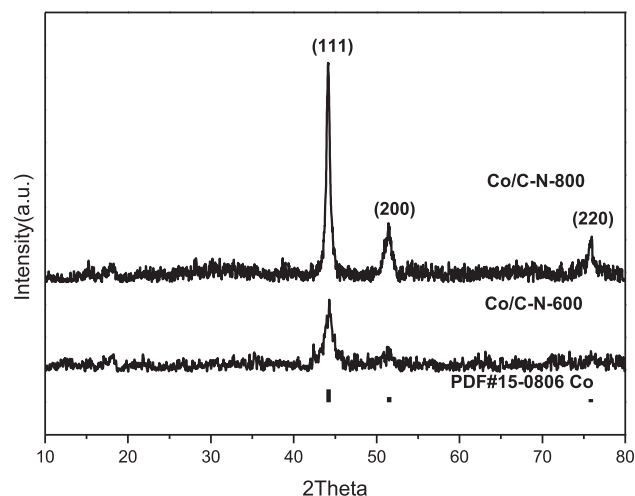


Fig. 1. XRD patterns of Co/C-N catalysts.

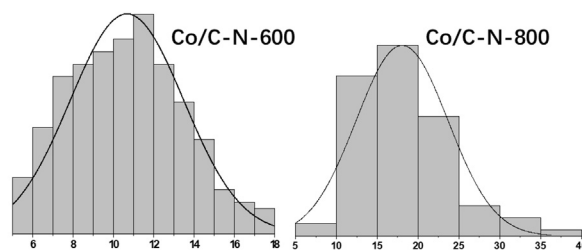
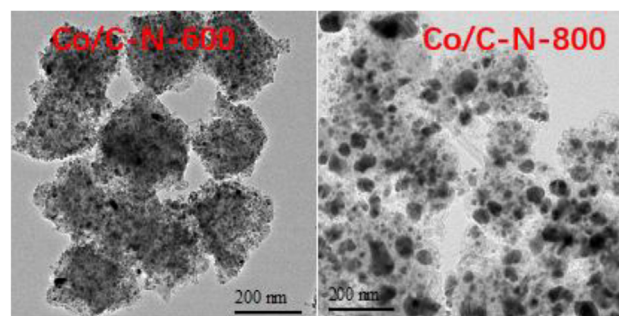


Fig. 2. TEM images and particle distribution of Co/C-N catalysts.

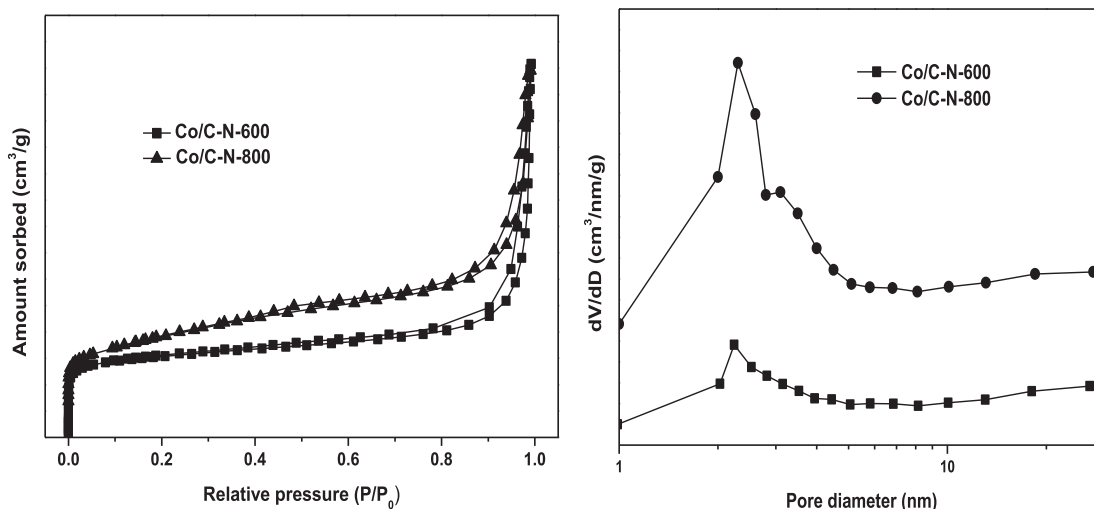


Fig. 3.  $N_2$  adsorption-desorption isotherms and pore size distribution curves of Co/C-N catalysts.

44.2°, 51.5°, 75.9°, which were assigned to the (1 1 1), (2 0 0), and (2 2 0) crystalline planes of metallic face-centered cubic (FCC) Co (JCPDS Card No. 15-0806) respectively. The size of Co metallic particles was calculated from the XRD peak (44.2°) using the Scherrer equation. The calculated crystallite sizes of Co were 11.5 nm and 17.8 nm for the Co/C-N-600 and Co/C-N-800, respectively.

The morphology of the Co/C-N was characterized with TEM. As shown in Fig. 2, the metallic Co was well dispersed on nitrogen doping carbon material. The average size of metallic Co was 12 and 18 nm for Co/C-N-600 and Co/C-N-800 according to the statistics of more than 200 Co particles. This result was quite consistent with the XRD calculations.

The  $N_2$  absorption isotherms of Co/C-N catalysts are shown in Fig. 3. The quantity of adsorbed  $N_2$  increased dramatically at a low relative pressure ( $P/P^0 < 0.08$ ), indicating the abundance of

Table 1  
The physical structure of Co/C-N catalysts.

Catalysts	Surface area ( $m^2/g$ )		Pore volume ( $mL/g$ )		Pore diameter (nm)	
	micro	meso	micro	meso	micro	meso
Co/C-N-600	231	289	0.097	0.45	0.48	2.03
Co/C-N-800	130	237	0.070	0.45	0.54	2.03

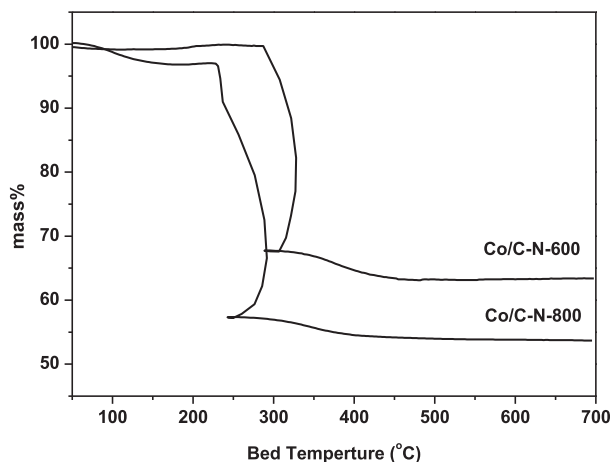


Fig. 4. TGA curves of Co/C-N catalysts.

micropores in the samples [12]. At the tail of the isotherm (high relative pressure), the absorbance increased quickly, suggesting a large amount of mesopores. It confirmed the dual mesoporous and microporous structure in Co/C-N materials [13]. With the increase of calcination temperature from 600 to 800 °C, the surface areas and micropore volumes of these two samples were found to decrease, while the micropore diameter increased slightly (Table 1).

Fig. 4 shows the TGA curves of Co/C-N catalysts. It could be seen that Co/C-N catalysts undergoes a two-step degradation process. The weight loss at about 100–250 °C should be ascribed as a result of dehydration of water from the crystalline structure. The weight loss at about 250–350 °C belonged to the oxidation of carbon and nitrogen materials [14]. The Co contents calculated from the weight loss were about 40% and 47% for Co/C-N-600 and Co/C-N-800.

The catalytic performance of Co/C-N was evaluated by the  $CO_2$  hydrogenation reaction at 200 and 220 °C successively. The product selectivity and STY of methanol are shown in Fig. 5 and Table 2, respectively. No deactivation of any catalysts, after 50 h of reaction, was observed under the testing conditions. It was noted that Co/C-N-600 had higher  $CO_2$  conversion than Co/C-N-800 at both 200 °C and 220 °C, because Co/C-N-600 had smaller Co particle size and thus more metallic Co active sites. The STY of methanol for Co/C-N-600 was also higher than

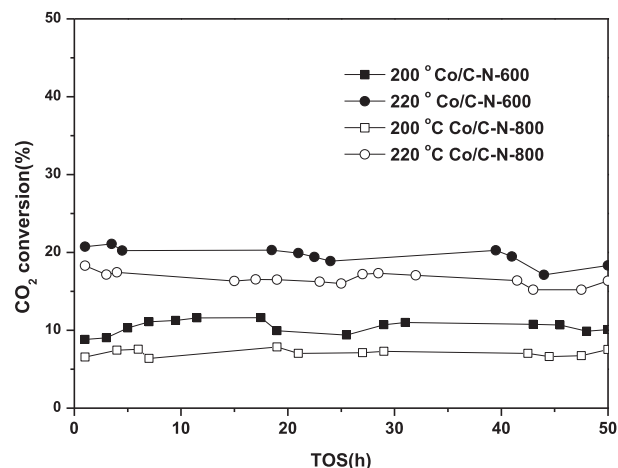
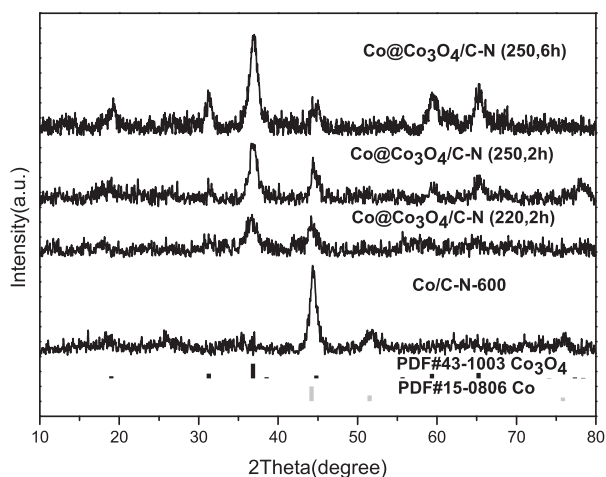


Fig. 5. Effect of temperature on  $CO_2$  conversion over the Co/C-N catalysts. Reaction conditions:  $P = 2$  MPa,  $GHSV = 6$   $L\ h^{-1}\ g_{cat}^{-1}$ ,  $H_2/CO_2 = 3$ .

**Table 2**

The activity and selectivity of Co/C-N catalyst.

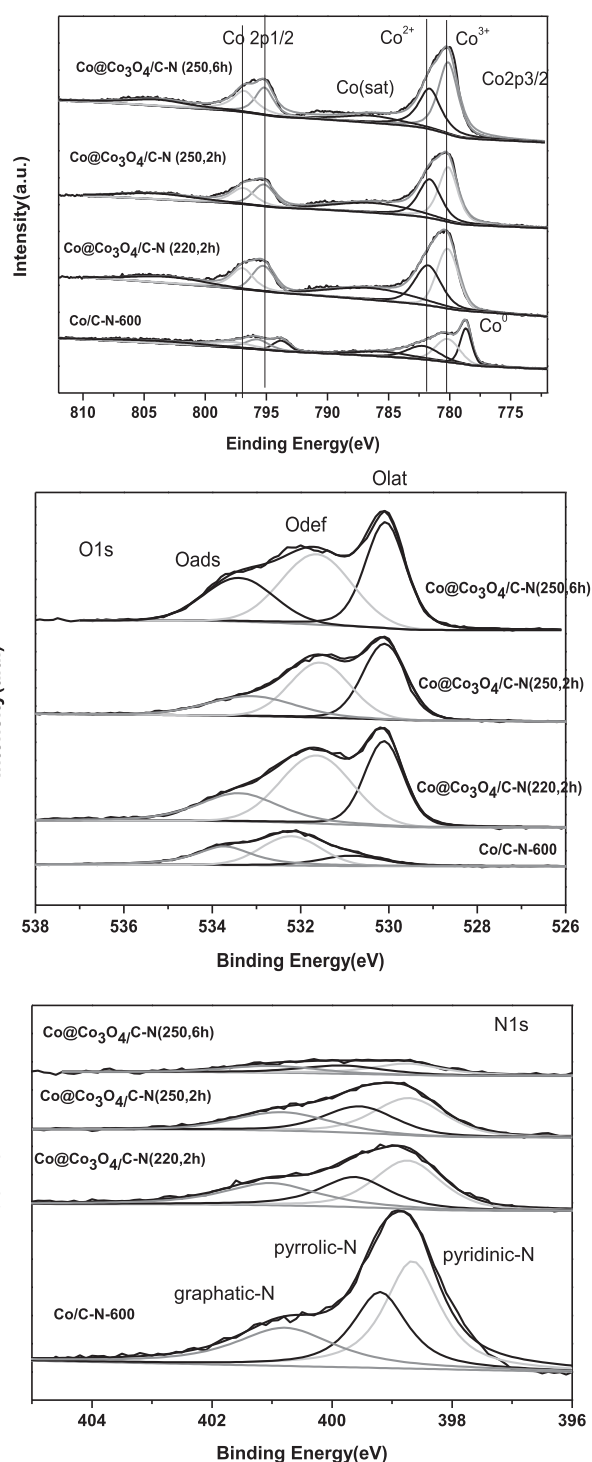
Catalyst	Reaction temperature (°C)	CO <sub>2</sub> conversion (%)	Selectivity (%)					STY <sub>MeOH</sub> (mmol/g <sub>cat</sub> /h)
			CO	CH <sub>4</sub>	C <sub>2</sub> H <sub>6</sub>	MeOH	EtOH	
Co/C-N-600	200	10.6	0	70.4	0.6	27.8	1.2	1.8
Co/C-N-600	220	19.4	0	85.7	0.6	12.6	1.1	1.5
Co/C-N-800	200	7.3	0	74.4	0.7	21.4	3.5	0.9
Co/C-N-800	220	16.6	0	80.5	0.7	15.3	3.5	1.5

**Fig. 6.** XRD patterns of Co/C-N and Co@Co<sub>3</sub>O<sub>4</sub>/C-N catalysts.

Co/C-N-800. Furthermore, as the reaction temperature increased from 200 °C to 220 °C, CO<sub>2</sub> conversion increased notably while the selectivity of methanol decreased. Since the methanol synthesis from CO<sub>2</sub> hydrogenation is exothermic, low temperature's should thermodynamically favorable in the conversion of CO<sub>2</sub>. However, the actual CO<sub>2</sub> conversion was much lower than the theoretical equilibrium value. Thus, CO<sub>2</sub> conversion was mainly affected by dynamic factors. Although metallic Co led to superior CO<sub>2</sub> conversion, it produced methane predominately in the process of CO<sub>2</sub> hydrogenation. There was no CO produced in all Co/C-N catalysts, while little ethane and ethanol, if any, was found in both gas and liquid products.

Co/C-N-600 was oxidized in air at different conditions to obtain different oxidation states. XRD patterns of Co/C-N, Co@Co<sub>3</sub>O<sub>4</sub>/C-N were displayed in Fig. 6. Diffraction peaks of Co<sub>3</sub>O<sub>4</sub> (JCPDS PDF 43-1004), as well as that of metallic Co, were observed in Co@Co<sub>3</sub>O<sub>4</sub> catalysts. As expected, the percentage of Co<sub>3</sub>O<sub>4</sub> increased while that of metallic Co decreased with the increase of oxidation temperature and time.

Fig. 7 shows the XPS spectra of Co 2p, O 1s and N 1s of the Co@Co<sub>3</sub>O<sub>4</sub>/C-N catalysts. The Co 2p peak of Co/C-N-600 could be deconvoluted into three peaks with binding energies (BEs) at 778.3, 780.3 and 782.2 eV, corresponding to metallic cobalt, Co<sup>3+</sup> and Co<sup>2+</sup> respectively [15]. The percentages of cobalt in oxidation states increased with the increase of oxidation temperature and time, and metallic Co almost disappeared in Co@Co<sub>3</sub>O<sub>4</sub>/C-N (250, 6 h). The O 1s XPS spectrum could be fitted into three peaks at BEs about 530.1, 531.7 and 533.5 eV, corresponding to lattice oxygen, defect oxygen and adsorbed oxygen [16]. The oxygen defects on the surface improved the dissociation of CO<sub>2</sub> and tended to produce the desired alcohol species [17]. The N 1s XPS spectrum of Co/C-N-600 could be fitted into three peaks with BEs at 398.5, 399.5 and 400.8 eV, corresponding to pyridinic N, pyrrolic N and graphitic N, respectively [18]. Similarly, the N 1s of the Co@Co<sub>3</sub>O<sub>4</sub>/C-N

**Fig. 7.** XPS profiles of Co 2p, O1s and N1s of Co/C-N and Co@Co<sub>3</sub>O<sub>4</sub>/C-N catalysts.

could also be fitted into the same three peaks yet with gradually lower intensities than Co/N-C-600, suggesting that the nitrogen content decreased with the increase of oxidation temperature and time.

The morphology of the Co@Co<sub>3</sub>O<sub>4</sub>/C-N (250, 6 h) was characterized with TEM and HRTEM (Fig. 8). The lattice spaces of 0.28 and 0.46 nm corresponding to the (2 2 0) and (1 1 1) of Co<sub>3</sub>O<sub>4</sub> confirmed the existence of oxidized Co species.

CO<sub>2</sub>-TPD was employed to investigate the adsorption ability for CO<sub>2</sub> on Co/C-N and Co@Co<sub>3</sub>O<sub>4</sub>/C-N catalysts. As depicted in Fig. 9,

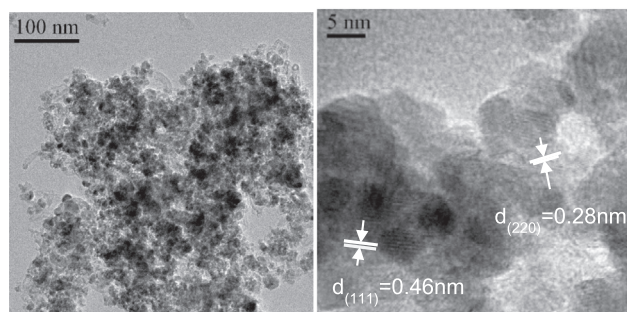


Fig. 8. TEM image and HRTEM image of Co@Co<sub>3</sub>O<sub>4</sub>/C-N (250, 6 h).

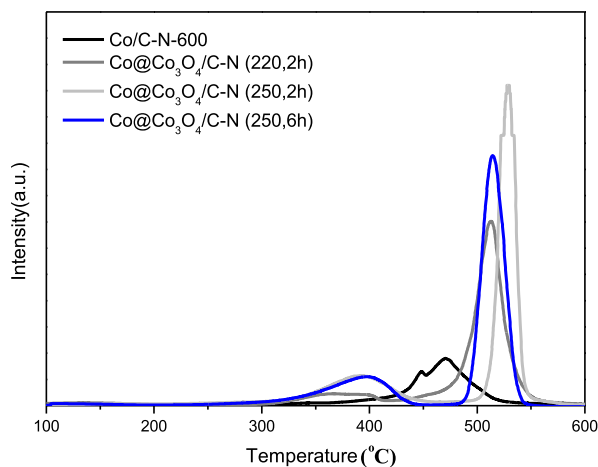


Fig. 9. CO<sub>2</sub>-TPD spectra of Co/C-N and Co@Co<sub>3</sub>O<sub>4</sub>/C-N catalysts.

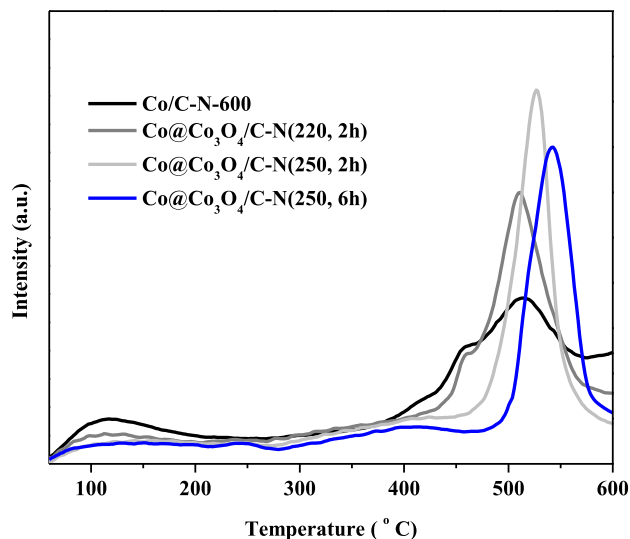


Fig. 10. H<sub>2</sub>-TPD spectra of Co/C-N and Co@Co<sub>3</sub>O<sub>4</sub>/C-N catalysts.

the Co/C-N catalyst showed two overlapping desorption peaks at 450 and 475 °C, which was ascribed to the chemisorbed CO<sub>2</sub> on the C-N support surface. Co@Co<sub>3</sub>O<sub>4</sub>/C-N catalyst showed two desorption at 400 °C and 500–550 °C, which were assigned to medium and strong basic sites, respectively [19]. The larger amount of adsorbed CO<sub>2</sub> of Co@Co<sub>3</sub>O<sub>4</sub>/C-N than that of Co/C-N at high temperature, indicative of the more basic sites on former catalyst surface, which was consistent with the N1s results in XPS profiles. High-temperature desorption property also indicates the existence of stronger metal–metal oxide (Co–Co<sub>3</sub>O<sub>4</sub>) interactions in Co@Co<sub>3</sub>O<sub>4</sub>/C-N [20].

All H<sub>2</sub>-TPD of the Co/C-N and Co@Co<sub>3</sub>O<sub>4</sub>/C-N catalysts (Fig. 10) showed two major peaks: a low temperature peak (<200 °C) and a high temperature peak (>400 °C), indicating different adsorbed states of hydrogen. The low temperature peak was ascribed to chemisorbed hydrogen on the metal Co surface, while the high temperature peak located at about 520 °C was probably caused by the desorption of spillover hydrogen from metallic Co to Co<sub>3</sub>O<sub>4</sub> [21]. The intensity of low temperature peaks, as well as the desorption temperature of high temperature peaks, decreased with the increase of oxidation temperature and time. It confirmed that the oxidation treatment decreased the amount of dissociative H<sub>2</sub> on metallic Co and increased the interaction between metallic Co and Co<sub>3</sub>O<sub>4</sub>, inducing H<sub>2</sub> desorption to much higher temperature.

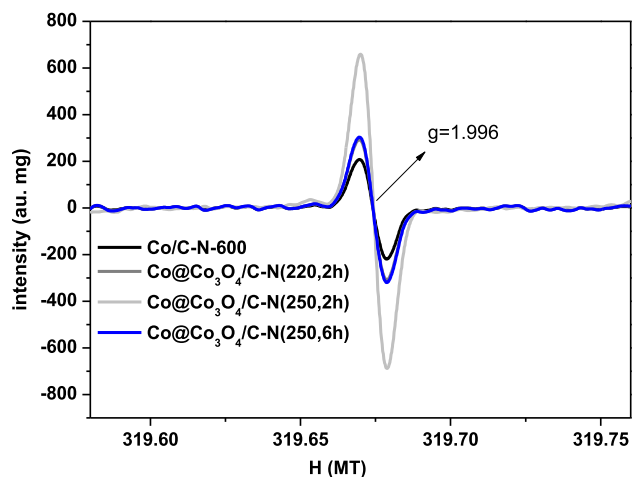


Fig. 11. ESR spectra of Co/C-N and Co@Co<sub>3</sub>O<sub>4</sub>/C-N catalysts.

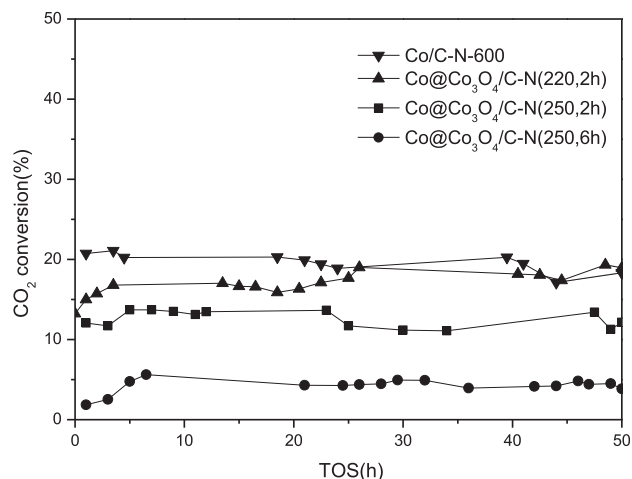


Fig. 12. Effect of temperature on CO<sub>2</sub> conversion over Co/C-N and Co@Co<sub>3</sub>O<sub>4</sub>/C-N catalysts. Reaction conditions: P = 2 MPa, T = 220 °C, GHSV = 6 L h<sup>-1</sup> g<sub>cat</sub><sup>-1</sup>, H<sub>2</sub>/CO<sub>2</sub> = 3.

**Table 3**The activity and selectivity of Co/C-N and Co@Co<sub>3</sub>O<sub>4</sub>/C-N catalysts.

Catalyst	CO <sub>2</sub> conversion (%)	Selectivity (%)					STY <sub>MeOH</sub> (mmol/g <sub>cat</sub> /h)
		CO	CH <sub>4</sub>	C <sub>2</sub> H <sub>6</sub>	MeOH	EtOH	
Co/C-N-600	19.4	0	85.7	0.6	12.5	1.2	1.5
Co@Co <sub>3</sub> O <sub>4</sub> /C-N (220, 2 h)	18.6	0	79.5	0.7	18.3	1.2	2.0
Co@Co <sub>3</sub> O <sub>4</sub> /C-N (250, 2 h)	13.5	0	79.7	0.8	18.7	0.8	1.5
Co@Co <sub>3</sub> O <sub>4</sub> /C-N (250, 6 h)	4.4	1.3	55.1	0.8	39.8	3.0	1.1

The formation of oxygen vacancy on the surface of Co@Co<sub>3</sub>O<sub>4</sub>/C-N is confirmed by the electron paramagnetic resonance (EPR) spectra of the samples, where the strong signal centering at  $g = 1.996$  originates from the Overlapped electrons. The ESR signals of Co@Co<sub>3</sub>O<sub>4</sub>/C-N catalysts increased with the increase of oxidation temperature and time in Fig. 11. Since oxygen vacancy with unpaired electrons is the main reason of the ESR response in these materials, the higher intensity of ESR signal indicated the occurrence of more defects formed in Co@Co<sub>3</sub>O<sub>4</sub>/C-N catalysts [22].

The values of CO<sub>2</sub> conversion, product selectivity and STY of methanol were shown in Fig. 12 and Table 3, respectively. Compared with Co/C-N-600, CO<sub>2</sub> conversion dropped, while selectivity of methanol increased with the decrease of metallic Co. Especially for Co@Co<sub>3</sub>O<sub>4</sub>/C-N (250, 6 h), CO<sub>2</sub> conversion dropped from 19.4% to 4.4%, however, the selectivity of methanol significantly increased from 12.5% to 39.8%. CO<sub>2</sub> conversion was directly related to the content of available sites of metallic Co due to its supply of dissociative hydrogen on the surface [7]. On the other hand, the selectivity of methanol was related to the oxygen defects in Co<sub>3</sub>O<sub>4</sub>, resulted in the partial oxidation of Co during heat treatment in air, which was consistent with the H<sub>2</sub>-TPD and ESR results. Balancing both factors, the highest STY of methanol (2.0 mmol/g<sub>cat</sub>/h) was obtained on Co@Co<sub>3</sub>O<sub>4</sub>/C-N (220,2h).

#### 4. Conclusion

Co/C-N materials were synthesized by calcination of ZIF-67 in N<sub>2</sub> atmosphere, while Co@Co<sub>3</sub>O<sub>4</sub>/C-N catalysts were prepared with partially oxidized Co/C-N in air at different conditions. The two series of catalysts were tested in the reaction of CO<sub>2</sub> hydrogenation. Characterization and catalytic evaluation showed that the metallic Co was the main activity site for CO<sub>2</sub> hydrogenation to methane due to the supply of dissociative hydrogen on the surface. Partial oxidation of Co/C-N decreased the content of metallic Co, weakening the strong ability to supply dissociative H<sub>2</sub>, and thus decreased the CO<sub>2</sub> conversion while increased methanol selectivity. The oxygen defects in Co@Co<sub>3</sub>O<sub>4</sub>/C-N improved the dissociation of CO<sub>2</sub> and tended to produce desired alcohol species. The highest yield of MeOH was obtained as 2.0 mmol g<sup>-1</sup> h<sup>-1</sup> over Co@Co<sub>3</sub>O<sub>4</sub>/C-N (220, 2 h) at 220 °C.

#### Acknowledgments

This project was supported by the Fundamental Research Funds for the Central University, China (CZT19007).

#### References

- [1] W. Wang, S.P. Wang, X.B. Ma, J.L. Gong, Chem. Soc. Rev. 40 (2011) 3703–3727.
- [2] A. Bansode, A. Urakawa, J. Catal. 309 (2014) 66–70.
- [3] J. Graciani, K. Mudiyansele, F. Xu, A.E. Baber, J. Evans, S.D. Senanayake, D. Stacchiola, P. Liu, J. Hrbek, J.F. Sanz, J.A. Rodriguez, Science 345 (2014) 546–550.
- [4] C.S. Li, G. Melaet, W.T. Ralston, K. An, C. Brooks, Y.F. Ye, Y.S. Liu, J.F. Zhu, J.H. Guo, S. Alayoglu, G.A. Somorjai, Nat. Commun. 6 (2015) 6538–6542.
- [5] A.G. Trencó, E.R. White, A. Regoutz, D.J. Payne, M.S.P. Shaffer, C.K. Williams, ACS Catal. 7 (2017) 1186–1196.
- [6] E.L. Kunkes, F. Studt, F. Abild-Pedersen, R. Schlögl, M. Behrens, J. Catal. 328 (2015) 43–48.
- [7] M. Schubert, S. Pokhrel, A. Thomé, V. Zielasek, T.M. Gesing, F. Roessner, L. Mädlerbe, M. Bäumer, Catal. Sci. Technol. 6 (2016) 7449–7460.
- [8] G. Melaet, W.T. Ralston, C.S. Li, S. Alayoglu, K.J. An, N. Musselwhite, B. Kalkan, G.A. Somorjai, J. Am. Chem. Soc. 136 (2014) 2260–2263.
- [9] B. Liu, B. Ouyang, Y.H. Zhang, K.L. Lv, Q. Li, Y.B. Ding, J.L. Li, J. Catal. 366 (2018) 91–97.
- [10] P. Zhou, C.L. Yu, L. Jiang, K.L. Lv, Z.H. Zhang, J. Catal. 352 (2017) 264–273.
- [11] Q.F. Deng, L. Liu, X.Z. Lin, G.H. Du, Y.P. Liu, Z.Y. Yuan, Chem. Eng. J. 203 (2012) 63–70.
- [12] X.B. Yang, J. Chen, Y.Q. Chen, P.J. Feng, H.X. Lai, J.T. Li, X.T. Luo, Nano-Micro Lett. 10 (2018) 15–25.
- [13] A. Schejn, A. Aboulaich, L. Balan, V. Falk, J. Lalevée, G. Medjahdi, L. Arand, K.M. R. Schneider, Catal. Sci. Technol. 5 (2015) 1829–1939.
- [14] K.Y.A. Lin, B.C. Chen, Dalton Trans. 45 (2016) 3541–3551.
- [15] A. Aijaz, J. Masa, C. Rçsler, W. Xia, P. Weide, A.J.R. Botz, R.A. Fischer, W. Schuhmann, M. Muhler, Angew. Chem. Int. Ed. 55 (2016) 4087–4091.
- [16] J. Díez-Ramírez, P. Sánchez, V. Kyriakou, S. Zafeiratos, G.E. Marnellos, M. Konsolakis, F. Dorado, J. CO<sub>2</sub> Util. 21 (2017) 562–571.
- [17] Z.H. He, Q.L. Qian, J. Ma, Q.L. Meng, H.C. Zhou, J.L. Song, Z.M. Liu, B.X. Han, Angew. Chem. Int. Ed. 55 (2015) 737–741.
- [18] H.G. Zhang, S. Hwang, M.Y. Wang, Z.X. Feng, S. Karakalos, L.L. Luo, Z. Qiao, X.H. Xie, C.M. Wang, D. Su, Y.Y. Shao, G. Wu, J. Am. Chem. Soc. 139 (2017) 14143–14149.
- [19] Y.W. Zhou, Y.X. Jiang, Z.Z. Qin, Q.R. Xie, H.B. Ji, Chin. J. Chem. Eng. 26 (2018) 768–774.
- [20] G.C. Yin, X.T. Yuan, X.L. Du, W. Zhao, Q.Y. Bi, F.Q. Huang, Chem. Eur. J. 24 (9) (2018) 2157–2163.
- [21] D.Y. Xu, W.Z. Li, H.M. Duan, Q.J. Ge, H.Y. Xu, Catal. Lett. 102 (2005) 229–235.
- [22] Z.C. Wang, W.J. Xu, X.K. Chen, Y.H. Peng, Y.Y. Song, C.X. Lv, H.L. Liu, J.W. Sun, D. Yuan, X.Y. Li, X.X. Guo, D.J. Yang, L.X. Zhang, Adv. Funct. Mater. doi: 10.1002/adfm.201902875.